

## A specialised delivery system for stratospheric sulphate aerosols design and operation

Janssens, M.; de Vries, I. E.; Hulshoff, S. J.

10.1007/s10584-020-02740-3

**Publication date** 

**Document Version** Final published version

Published in Climatic Change

Janssens, M., de Vries, I. E., & Hulshoff, S. J. (2020). A specialised delivery system for stratospheric sulphate aerosols: design and operation. *Climatic Change*, *162*(1), 67-85. https://doi.org/10.1007/s10584-020-02740-3

Important note

To cite this publication, please use the final published version (if applicable). Please check the document version above.

Other than for strictly personal use, it is not permitted to download, forward or distribute the text or part of it, without the consent of the author(s) and/or copyright holder(s), unless the work is under an open content license such as Creative Commons.

Takedown policy

Please contact us and provide details if you believe this document breaches copyrights. We will remove access to the work immediately and investigate your claim.

# A specialised delivery system for stratospheric sulphate aerosols: design and operation



M. Janssens<sup>1</sup> · I. E. de Vries<sup>2</sup> · S. J. Hulshoff<sup>1</sup> · DSE 16-02

Received: 24 July 2019 / Accepted: 14 May 2020 / Published online: 02 August 2020 © The Author(s) 2020

#### Abstract

Temporary stratospheric aerosol injection (SAI) using sulphate compounds could help to mitigate some of the adverse and irreversible impacts of global warming. Among the risks and uncertainties of SAI, the development of a delivery system presents an appreciable technical challenge. Early studies indicate that specialised aircraft appear the most feasible (McClelan et al., Aurora Flight Sciences, 2010; Smith and Wagner, Environ Res Lett 13(12), 2018). Yet, their technical design characteristics, financial cost of deployment, and emissions have yet to be studied in detail. Therefore, these topics are examined in this twopart study. This first part outlines a set of injection scenarios and proposes a detailed, feasible aircraft design. Part 2 considers the resulting financial cost and equivalent CO<sub>2</sub> emissions spanned by the scenarios and aircraft. Our injection scenarios comprise the direct injection of H<sub>2</sub>SO<sub>4</sub> vapour over a range of possible dispersion rates and an SO<sub>2</sub> injection scenario for comparison. To accommodate the extreme demands of delivering large payloads to high altitudes, a coupled optimisation procedure is used to design the system. This results in an unmanned aircraft configuration featuring a large, slender, strut-braced wing and four custom turbofan engines. The aircraft is designed to carry high-temperature H<sub>2</sub>SO<sub>4</sub>, which is evaporated prior to injection into a single outboard engine plume. Optimised flight profiles are produced for each injection scenario, all involving an initial climb to an outgoing dispersion leg at 20 km altitude, followed by a return dispersion leg at a higher altitude of 20.5 km. All the scenarios considered are found to be technologically and logistically attainable. However, the results demonstrate that achieving high engine plume dispersion rates is of principal importance for containing the scale of SAI delivery systems based on direct H<sub>2</sub>SO<sub>4</sub> injection, and to keep these competitive with systems based on SO<sub>2</sub> injection.

Design Synthesis Exercise 2016 - Group 02: M. Cruellas Bordes, C. J. G. De Petter, A. F. van Korlaar, L. P. Kulik, R. Maselis, L. H. Mulder, S. Stoev, K. J. F. van Vlijmen, C. H. Melo Souza, D. Rajpal

**Electronic supplementary material** The online version of this article (https://doi.org/10.1007/s10584-020-02740-3) contains supplementary material, which is available to authorized users.

S. J. Hulshoff s.j.hulshoff@tudelft.nl

Department of Meteorology (MISU), Stockholm University, Svante Arrheniusvägen 16, Stockholm, Sweden



Faculty of Aerospace Engineering, Delft University of Technology, Kluyverweg 1, Delft, Netherlands

**Keywords** Climate engineering · Solar geoengineering · Solar radiation management · Stratospheric sulphate aerosol injection · Technological implementation · Specialised aircraft

#### 1 Introduction

There is broad scientific consensus on the causes of global warming (Cook et al. 2013) and on the necessary solution: Achieving net zero greenhouse gas (GHG) emissions and removing excess GHGs from the atmosphere. This may take a considerable amount of time, however, as significant GHG emission reductions require large changes to the current industrial, agricultural, transportation and energy production infrastructure (Clarke et al. 2014), while efficient carbon capture techniques have yet to be developed. GHG concentrations and associated warming might therefore proceed along a high Representative Concentration Pathway (RCP), as introduced in (IPCC 2013). In such a scenario, the probability and severity of adverse and irreversible impacts from continued climate change increases progressively (IPCC 2018). To help alleviate these dangers, decarbonising efforts might be temporarily complemented by additional measures, such as Solar Radiation Management (SRM). We emphasise that although SRM might be justified as a temporary emergency intervention, it cannot be considered to be part of the solution to climate change. It must thus not distract from the main focus: reducing global GHG concentrations by achieving net zero emissions and GHG removal. Still, SRM's potential effectiveness as a complementary measure demands a more detailed assessment of its risks and benefits. In this paper, we therefore contribute to the assessment of Stratospheric Aerosol Injection (SAI) (Crutzen 2006), generally acknowledged to be the most feasible SRM option (Shepherd 2009).

Due to the environmental and societal risks and uncertainties associated with SRM, a large number of political and ethical aspects must be thoroughly addressed before a decision on the viability of SAI can be made (Robock 2014). The technical implementation of SAI is also associated with risks and uncertainties, as it requires the delivery of large payloads (in this context, large masses of aerosols or their precursors) to altitudes far higher than those flown at by conventional aircraft. Therefore, it is also necessary to estimate the feasibility, implementation time, financial cost of deployment and GHG emissions of any potential SAI delivery system.

While various delivery systems have been considered (Davidson et al. 2012; Robock 2014), we focus on systems based on aircraft. The use of existing aircraft and specially designed aircraft were contrasted in (McClellan et al. 2010). They concluded that due to the narrow technical operating window associated with stratospheric flight, specialised aircraft are likely cheaper and easier to operate successfully. This is corroborated by a recent survey of aerospace design companies on the feasibility of employing their existing aircraft (Smith and Wagner 2018), which finds that specialised aircraft are likely the only feasible alternative. However, as both studies were preliminary in their technical analysis, there remains considerable uncertainty in the technical design aspects of specialised aircraft, leading to widely varying cost estimates (Smith and Wagner 2018).

In order to reduce uncertainty associated with the use of a fleet of specialised aircraft for SAI, Part 1 of this series considers the design and operation of such a delivery system in more detail. Emphasis is placed on solutions with a high technological readiness level. Part 2 of this series addresses the initial and operating financial cost and equivalent CO<sub>2</sub> emissions of the delivery system. It also considers the sensitivities of these quantities to a number of external factors.



In the following sections, we first describe the selection of an aerosol compound, the injection strategies and four possible injection scenarios. Then, the factors influencing aircraft design in the context of SAI are discussed. Next, a coupled aircraft-operation design procedure is described and complete feasible delivery systems are presented and briefly discussed for the four injection scenarios. Finally, the consequences of choosing alternatives for two key design options are quantified and discussed.

## 2 Aerosol and delivery requirements

## 2.1 Selection of aerosol precursor

Some of the anticipated risks of SAI, including ozone loss, stratospheric heating, increased diffuse radiation and acid deposition might be reduced by using aerosols based on engineered solid particles. Calcite, alumina and diamond particles, for example, have a high refractive index and might reduce forward scattering (Pope et al. 2012; Weisenstein et al. 2015; Dykema et al. 2016) and the use of alkaline metal salts such as CaCO<sub>3</sub> might counteract ozone depletion due to acid neutralisation on their outer surface (Keith et al. 2016). However, significant unknowns remain in the use of engineered aerosols. These pertain to their implementation, e.g. the technology and injection strategy for successful aerosol formation, and to their impacts, e.g. possible chemical interactions with stratospheric compounds and their influence on ecosystems once deposited (Pope et al. 2012; Weisenstein et al. 2015).

An alternative is to use sulphate aerosols. The physical properties and costs of sulphur are well known, and their background presence in the atmosphere due to volcanic and industrial emissions allows rough estimations of their side effects and radiative forcing (Crutzen 2006; Pope et al. 2012). These estimates are still imprecise, as the altitudes and particle sizes considered in current SAI scenarios differ from those associated with volcanic and industrial sources. The resulting uncertainties, however, are generally considered to be far less than those associated with engineered aerosols.

Sunlight-scattering sulphate aerosols in the stratosphere consist of particles mostly comprised of aqueous  $H_2SO_4$ . These can be introduced into the atmosphere either by injection of precursor compounds or by direct injection of  $H_2SO_4$ . The injection of precursor compounds, such as  $SO_2$ , is potentially advantageous from the storage point of view, due to their mild corrosion characteristics and lower net weight. However, in the atmosphere  $SO_2$  oxidises to form  $H_2SO_4$  only after a relatively long time of  $\approx 40$ –50 days (Tilmes et al. 2017; Vattioni et al. 2019), meaning that the conditions of sulphate aerosol formation cannot be controlled. Injection of  $SO_2$  typically leads to particles that are larger than optimal and therefore are less effective scatterers and have shorter stratospheric residence times (e.g., Pierce et al. 2010). The slow conversion of  $SO_2$  into  $H_2SO_4$  also means that a substantial part of the injected sulphur in the stratosphere is not in sulphate aerosol form. With  $SO_2$  as the injection species, on average more than one-eighth of the annually injected sulphur mass is present in form of  $SO_2$  and is thus ineffective. Furthermore, not all injected  $SO_2$  oxidises to  $H_2SO_4$ ; a part of the precursor mass is removed from the stratosphere by diffusion and mixing without having undergone oxidation and aerosol formation at all (Vattioni et al. 2019).

In contrast, the direct injection of  $H_2SO_4$  in gas phase facilitates directing the initial particle formation process (Pierce et al. 2010; Benduhn et al. 2016). In conditions where particle growth is self-limited and independent of nucleation rate, particle sizes are determined by the initial  $H_2SO_4$  concentration and the diffusivity of the background flow in



which it is injected (Benduhn et al. 2016; Turco and Yu 1997). Direct  $H_2SO_4$  injection targeting an initial particle radius of approximately 0.1  $\mu$ m is expected to lead to a favourable aerosol size distribution throughout the aerosol's stratospheric residence time (Pierce et al. 2010; Benduhn et al. 2016), which allows irradiation reduction to be increased by 17–70%, depending on injection details, relative to that obtained by injection of  $SO_2$  (Vattioni et al. 2019). The aerosol distribution of directly injected  $H_2SO_4$  derives its stronger irradiation reduction from containing larger numbers of smaller particles. Yet, this also leads to a larger total particle surface area. This has the disadvantage of increasing adverse effects associated with stratospheric sulphate aerosol presence, such as ozone depletion and stratospheric warming (Pope et al. 2012; Heckendorn et al. 2009). However, the increased scattering efficiency due to particle diameter decrease outweighs the increased adverse effects, as shown by (Vattioni et al. 2019). This implies that direct  $H_2SO_4$  injection under ideal circumstances can achieve a given negative radiative forcing target with lower annual sulphur delivery rate and less adverse effects than  $SO_2$  injection.

In all, direct  $H_2SO_4$  injection appears promising with respect to  $SO_2$  injection, though direct comparisons are relatively sparse and significant uncertainties remain. Still, the apparent benefits of direct  $H_2SO_4$  injection lead us to mainly focus on this scenario for our aircraft-based delivery system. We will assume that the  $H_2SO_4$  is transported in liquid phase, due to a lack of proven technology for in-flight  $H_2SO_4$  production from precursors (Smith et al. 2018). This necessitates the use of an evaporation system to ensure that the  $H_2SO_4$  is injected as a condensable gas. The temperature of the engine exhaust flow in which the  $H_2SO_4$  gas is injected may be high enough to enable simultaneous evaporation and injection, eliminating the need for a separate evaporation system. However, because the injection specifics are very important for aerosol particle formation, as outlined below, we assume a conservative configuration including an evaporation system.

As mentioned, direct H<sub>2</sub>SO<sub>4</sub> vapour injection only allows indirect control of particle formation via nucleation, condensation and coagulation. To obtain more direct control of particle size, these formation processes would have to be eliminated or completed in a controlled environment inside the aircraft. To our knowledge, however, no spray technology to reliably produce ideally sized droplets at high enough rates exists (Technical and Business Development Director Micron Sprayers Ltd., personal communication, Nov 4, 2019) and it is unlikely that the circumstances needed to allow automated and controlled nucleation, condensation and coagulation to take place can readily be created inside an aircraft. Therefore, we base our injection strategy on the existing literature on aerosol formation by condensation of gas phase H<sub>2</sub>SO<sub>4</sub> injection into an expanding plume.

## 2.2 Delivery rates and location

Specifying the goal of potential SAI is not trivial, and different focus parameters can be chosen, such as e.g. global average temperature reduction, warming rate reduction, regional temperature reductions or average radiative forcing. In the latter case, the target negative radiative forcing could be based on the current positive radiative forcing with respect to preindustrial times, or roughly 2.5 to 3 Wm<sup>-2</sup> (IPCC 2018). To provide conservative measures of the costs and emissions of an SAI delivery system, such a mission objective will be considered in the present study. This corresponds to an annual delivery rate of 15 Mt H<sub>2</sub>SO<sub>4</sub> year<sup>-1</sup> (5 Mt S year<sup>-1</sup>) (Pierce et al. 2010).

This study assumes that the delivery takes place at altitudes near 20 km. This is sufficiently far above the tropopause to prevent mixing of aerosols into the troposphere and



fast sedimentation (Rasch et al. 2008; Pierce et al. 2010). Even though an increased coagulation rate reduces the efficiency of individual particles if injected above 20 km, higher injection altitudes will still yield a more effective irradiation reduction, given the resulting longer residence time of the aerosols (Tilmes et al. 2017; Vattioni et al. 2019). However, as will be discussed in Sections 3 and 5, delivery at altitudes higher than 20 km is likely to be unfeasible.

Injection latitudes near 15° North and South will be assumed, as these have been shown to be favourable for global aerosol coverage and stratospheric residence times (Tilmes et al. 2017; Vattioni et al. 2019). It may be assumed that a steady state of aerosol coverage and optical depth is reached after approximately two years (Tilmes et al. 2017; Reed 1966; Uppala et al. 2005).

As described in the next section, the rate at which  $H_2SO_4$  can be delivered within a single flight is dependent on the technology employed. Consequently, three  $H_2SO_4$  injection scenarios will be examined. For comparison, we will also examine a scenario in which only  $SO_2$  is delivered, at annual delivery rates sufficient to produce equivalent negative short-wave radiative forcing.

## 2.3 H<sub>2</sub>SO<sub>4</sub> dispersion rate (DR)

Two parameters driving the production of optimally sized particles from direct  $H_2SO_4$  vapour injection are the initial  $H_2SO_4$  concentration and background flow diffusivity. According to Benduhn et al. (2016), initial concentrations suitable for expanding aircraft engine plumes vary between  $3 \cdot 10^{15}$  and  $10^{18}$  molecules  $H_2SO_4$  cm<sup>-3</sup> (Benduhn et al. 2016) (or  $C_{init} = 0.0005 - 0.2$  kgm<sup>-3</sup>). Maintaining initial concentrations near the lower limit of this interval requires low injection rates and correspondingly long flight times, which substantially increases the costs associated with delivery. On the other hand, the use of high initial concentrations requires high engine plume diffusivities. Currently the maximum achievable levels of diffusivity in stratospheric engine plumes can only be estimated. To deal with this uncertainty, we examine three direct  $H_2SO_4$  injection scenarios. These differ most crucially in terms of their implied dispersion rates (DR).

The dispersion rate DR in kg H<sub>2</sub>SO<sub>4</sub>m<sup>-1</sup>, for the injection of H<sub>2</sub>SO<sub>4</sub> at a rate  $\dot{m}$  kg s<sup>-1</sup>, into an engine plume with a volume flow  $\dot{V}$  m<sup>3</sup>s<sup>-1</sup> emitted from an aircraft travelling at speed  $v_{ac}$  ms<sup>-1</sup> is given by:

$$DR = \frac{\dot{m}}{v_{ac}} = \frac{C_{init}\dot{V}}{v_{ac}} \tag{1}$$

This assumes that the  $H_2SO_4$  concentration,  $C_{init}$ , is uniform within the plume. The total aircraft payload delivered is given by the value of DR integrated over the range of the flight.

Previous studies have assumed that constant, uniform diffusivities between  $10^2$  and  $10^3$  m<sup>2</sup>s<sup>-1</sup> can be maintained in an aircraft engine plume throughout the aerosol's early growth phase (a period on the order of seconds to minutes) (Pierce et al. 2010; Benduhn et al. 2016; Smith et al. 2018). However, aircraft engine plumes typically do not display constant, uniform background diffusivities. Normally the diffusivity declines in the initial minutes of particle growth, as energetic engine-driven mixing is gradually replaced by mixing at the much larger scales associated with wing tip vortices (Yu and Turco 1998; Schumann et al. 1998). The magnitude and distribution of diffusivity will thus depend on the specific details of the engine and aircraft configuration. To capture the effects of such variations, the three direct  $H_2SO_4$  injection scenarios considered below have been developed using different options for engine plume injection.



## 2.4 Core injection (CI) scenario

As will be discussed in Section 3, the scale of the intended mission justifies the development of a specialised turbofan engine. Turbofan engines have two different volume flows, the first associated with the warm, high-velocity engine core and the second associated with the cool, low-velocity outer bypass. For the first scenario, we assume that  $H_2SO_4$  is injected into the core flow only. This is chosen mainly because it is most consistent with plume models applied in literature (Pierce et al. 2010; Benduhn et al. 2016). We thus assume it achieves a diffusivity value of  $10^2 \, \mathrm{m}^2 \mathrm{s}^{-1}$ , similar to the value used by Yu and Turco (1998) and measured by Schumann et al. (1998). This is the most conservative of the scenarios considered, as it ignores the potential gains obtainable by also injecting into the bypass flow.

Targeting an initial particle radius of  $\approx 0.1~\mu m$  at the assumed diffusivity requires an initial  $\rm H_2SO_4$  concentration of approximately  $10^{16}~\rm cm^{-3}$  (Benduhn et al. 2016). For the specific aircraft design considered later in this paper, the core volume flow is 260 m³s<sup>-1</sup> at the high thrust settings necessary for stratospheric cruise. At the corresponding aircraft cruise speed of  $v_{ac} = 210~\rm ms^{-1}$ , the resulting dispersion rate is relatively low:  $DR = 0.002~\rm kgm^{-1}$ . This is more conservative than the value for the equal diffusivity and initial concentration used by Pierce et al. (2010), who assumed uniformly high diffusivities throughout the aircraft wake and a relatively large effective aerosol outlet area of 6 m², leading to a large volume flow for injection.

## 2.5 Full injection (FI) scenario

The outer bypass flow of the proposed turbofan engine can be expected to have relatively low values of diffusivity, owing to its relatively low velocities. However, as its volume flow is 7.5 times greater in magnitude than that of the core flow, it can help increase the DR to reduce required flight time. Thus, in the second scenario, injection into the full engine flow is considered. It is assumed that exhaust mixers are used to achieve a well-mixed and uniformly seeded initial plume. These are commonly employed in low-bypass turbofans (Larkin and Blatt 1984; Holzman et al. 1996) and some high-bypass turbofan engines (Mundt and Lieser 2001). The use of such mixers is a relatively conservative assumption, as lighter, but less proven alternatives exist, such as the use of overexpanded bypass flows. These show the potential for providing uniform mixing in the early plume at virtually no thrust penalty (Debiasi et al. 2007). Both conventional mixers and overexpanded bypass flows can be expected to have the additional advantage of reducing jet noise (Mundt and Lieser 2001).

Well-mixed early plumes have been found to display slightly higher diffusivities than core-only flows (Debiasi et al. 2007). Hence, it will be conservatively assumed that the mixed core and bypass flow approximately maintains the diffusivity value of  $10^2$  m<sup>2</sup>s<sup>-1</sup>. As for the first scenario, this requires an initial H<sub>2</sub>SO<sub>4</sub> concentration of approximately  $10^{16}$  cm<sup>-3</sup>. Owing to the higher total volume flow, however, the resulting dispersion in this scenario is DR = 0.02 kgm<sup>-1</sup>.

#### 2.6 Optimised full injection (OFI) scenario

The first two scenarios assume relatively conservative values of diffusivity. However, improved engine flow mixing technology or more accurate measurements and simulations of plume growth might show that higher values can be attained. Thus, the third scenario will consider the case where a relatively high value of diffusivity,  $3 \cdot 10^2$  m<sup>2</sup>s<sup>-1</sup>, is achieved in combination with both core and bypass injection. This corresponds to a much higher



initial  $H_2SO_4$  concentration of  $3 \cdot 10^{17}$  cm<sup>-3</sup>, which is still well within the desired aerosol regime described in Benduhn et al. (2016). The resulting dispersion rate,  $DR = 0.5 \text{ kgm}^{-1}$ , is substantially larger than those of the first two scenarios.

## 2.7 Precursor gas (SO<sub>2</sub>) injection scenario

When precursors such as SO<sub>2</sub> are injected, aerosol formation does not occur until long after delivery and is thus virtually independent of injection specifics. In this case, the dispersion rate in flight is not constrained. This means cost-efficient, short, high-payload flights can be employed. Furthermore, recent studies have demonstrated that negative radiative forcing from point source injection of SO<sub>2</sub> at 20 km peaks for injection locations around 15° N and could achieve radiative forcing reductions of 2.5 to 3 Wm<sup>-2</sup> as well (Tilmes et al. 2017; MacMartin et al. 2017). However, due to the slow conversion to  $H_2SO_4$ , average particle sizes increase and scattering efficiency decreases. As a conservative estimate, we assume that approximately twice the amount of sulphur is required to achieve the same radiative forcing with SO<sub>2</sub> with respect to H<sub>2</sub>SO<sub>4</sub> injection, based on radiative forcing estimates from (Pierce et al. 2010; Tilmes et al. 2017). To assess the combined effects of the constrained DR but lower annual delivery requirement in H<sub>2</sub>SO<sub>4</sub> injection scenarios, a fourth, SO<sub>2</sub> precursor injection scenario will be examined ( $SO_2$ ). It assumes the delivery of 20 Mt  $SO_2$ y<sup>-1</sup> (10 Mt S) at the same altitudes and latitudes as the H<sub>2</sub>SO<sub>4</sub> scenarios, delivered in short-range flights from four airports approximating point sources. The top half of Table 2 summarises the most important differences between the four scenarios.

## 3 Aircraft design considerations

From the perspective of aircraft design, SAI poses a significant challenge, as it is dominated by the requirement to bring a substantial payload to unusually high altitudes, potentially covering substantial range. This differs from the combination of take-off, cruise and landing requirements that drive conventional aircraft design.

Decreasing air density becomes problematic above approximately 15 km, affecting both the wing's, affecting both the wing's ability to balance the weight of the aircraft, payload and fuel and the engines' ability to balance the aircraft's aerodynamic drag. Furthermore, there are requirements related to the safe operation of the aircraft which must be considered. The impact of these effects and requirements on the design of a specialised SAI aircraft are described below.

#### 3.1 Lift and drag at high altitudes

The total weight is balanced primarily by the lift produced by the wing, L which may be expressed as:

$$L = \frac{1}{2}\rho v_{ac}^2 A_w C_L \tag{2}$$

where  $\rho$  is the air density,  $A_w$  is the wing reference area and  $C_L$  is a non-dimensional coefficient dependent on the wing design and its operating conditions. Balancing the total weight at altitudes with small  $\rho$  requires high  $C_L$ , velocities or wing area. Wing size and shape is also a main contributor to aerodynamic drag D, given by:

$$D = \frac{1}{2}\rho v_{ac}^2 A_w C_d \tag{3}$$

where  $C_d$  is the non-dimensional drag coefficient of the aircraft. Since  $v_{ac}$  and/or  $A_w$  must be relatively large, there is significant impetus for reducing  $C_d$ .

A major component of  $C_d$ , known as induced drag, varies with  $C_L^2$ . Therefore, although D scales with  $A_w$ , it is beneficial to employ relatively large wing areas, as this reduces the required  $C_L$  and total D. The  $C_L$ -dependent component of  $C_d$  can also be reduced by using slender wings, with relatively high aspect ratio AR. Operating with slender wings at high speeds is particularly difficult, as these are relatively flexible. As the speed of the aircraft is increased, changes in aerodynamic load lead to increasingly large deflections. Ultimately, this can lead to dangerous static or dynamic aeroelastic modes, such as control reversal or flutter. This is particularly true if the aircraft is operating near the speed of sound, where phenomena associated with air compressibility, such as shock waves or shock-induced separation, introduce additional aeroelastic modes. The onset of such phenomena is a function of the Mach number M, defined by  $M = \frac{v_{ac}}{a}$  where a is the speed of sound. Generally, the need to avoid undesirable aeroelastic modes while maintaining low structural weight limits the maximum speed range of efficient designs to M < 0.8. Even with this restriction, excessive values of AR must be avoided.

The drag can in principle also be reduced by decreasing the thickness of the wing's airfoil section, avoiding a large rise in the  $C_d$  associated with higher M (known as drag divergence). In the current context, however, a relatively thick airfoil is required to maintain sufficient stiffness to support even a moderately large aspect ratio and prevent excessive induced drag. The final multidisciplinary design procedure, described in Section 4, resulted in a wing with a relatively thick airfoil (limited to M < 0.71), a moderate aspect ratio of AR = 13 and a large wing area of 700 m<sup>2</sup>, supported by a strut for additional stiffness. In spite of the multidisciplinary optimisation, the final estimated operating drag values are still appreciable.

## 3.2 Thrust at high altitudes

D must be balanced by the thrust T produced by the engines. Operating at low air density reduces both engine mass flow and combustion efficiency, yielding a strong thrust lapse with altitude. Thus, exceptionally powerful engines are required to sustain efficient flight at stratospheric altitudes. This is the driving constraint for the present design and requires turbojet, low-bypass turbofan or high-bypass turbofan engines (Torenbeek 2013).

The former two are generally superior in terms of thrust-to-weight ratio, while the latter generally achieves higher total thrust and lower fuel consumption per unit thrust. Turbojet engines are widely used in military aircraft, where long-term reliability is less important. For a SAI application, however, the thrust of the most common examples would likely need to be down-rated to maintain sufficient reliability. State-of-the-art low-bypass turbofans are used to power a number of low-weight aircraft to stratospheric altitudes and are therefore suggested for SAI application in Smith and Wagner (2018). However, their relatively high fuel consumption diminishes their weight advantage, especially if the aircraft must cover a substantial delivery range. Hence, high-bypass turbofans might be the more efficient alternative and will be the more environmentally friendly alternative.

There are few existing examples of high-altitude high-bypass turbofans. This means that a custom turbofan, developed specifically for a fleet of SAI aircraft at stratospheric altitudes, could be necessary. This would raise development costs. Nevertheless, the potential benefits of a custom engine mandate the inclusion of such a design within the current study. In Section 5 and in the supplementary material, we quantify the relative benefits of employing existing low-bypass turbofans, existing high-bypass turbofans and custom high-bypass turbofans for the proposed delivery system.

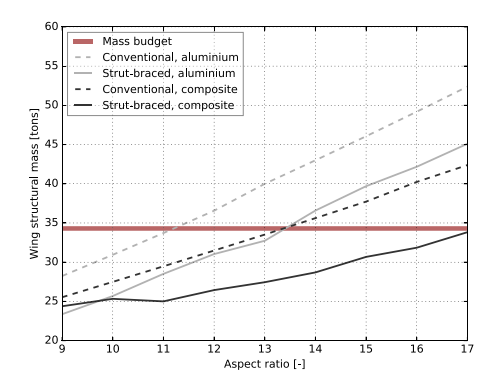


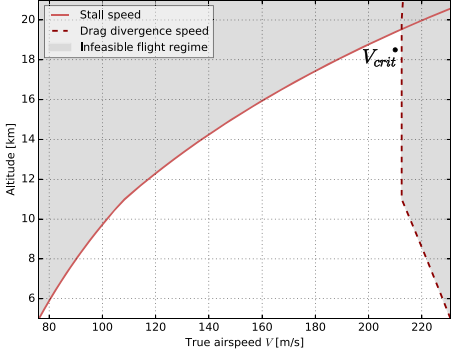
## 3.3 Additional requirements

Aside from being stiff enough to avoid undesirable aeroelastic modes, the aircraft structure must withstand several distinct load cases. These include the fully loaded case at take off, where flexibility and high fuel load can result in wing-ground strikes, and the near-empty case approaching the end of the flight, where the low wing weight due to depleted fuel and aerosol combined with the need to support the fuselage results in high wing-root bending moments in gust conditions. These and other requirements produce a trend of increasing structural weight with aspect ratio, as Fig. 1 shows for various wing configuration and material options. The figure shows how structural weight can be decreased by using composite materials instead of aluminium and an additional strut to support the main wing structure.

In spite of the fact that the aircraft will make use of automated control systems, a minimum level of handling qualities is required in order to ensure that the aircraft is stable and controllable. This determines the sizes of the vertical and horizontal tail surfaces, as well as those of the rudder, elevator and ailcron control surfaces.

Finally, the aircraft must be operated with sufficient margin from its altitude ceiling. A useful visualisation of this is a velocity-altitude plot. Figure 1 includes such a plot for the limiting stage of the flight profile discussed in Section 4.1. The left curve indicates the minimum operating speed, or stall speed, of the aircraft. Below this airspeed, lift is insufficient to sustain flight. The stall speed increases rapidly with altitude due to the rapid drop in air density. The right curve indicates the maximum operating speed at the drag divergence Mach number and the associated aeroelasticity and thrust boundary. It is necessary to operate below this speed to avoid excessive thrust requirements and undesirable aeroelastic phenomena as the flight speed approaches the local speed of sound. A critical area to be avoided is the intersection of the two curves, known as the "coffin corner", where there is little margin for operation.





(a) Total wing structural mass versus aspect ratio for unsupported and strut braced wings with boron fibre laminate composite and aluminium construction. The values shown are for the baseline aircraft design described in section 4.1.

(b) Graphical representation of the "coffin corner" for the aircraft presented in section 4.1 in its critical design state, where the range in airspeed providing sufficient lift to balance the weight lies in the triangle spanned by the curves and  $V_{crit}$  is the true air speed of the aircraft in this critical condition

Fig. 1 Constraints in high-altitude, high-payload aircraft design

## 4 Coupled aircraft/flight profile design

Due to the extreme operating altitudes required for SAI, flight profile parameters such as total (fuel and payload) mass, speed, range and altitude strongly influence the aircraft design requirements, while aircraft parameters such as wing geometry and structure strongly influence the achievable total mass, speed and altitude. Thus, in order to assure both the feasibility and relative efficiency of the aircraft configuration emerging from the design, a simultaneous optimisation of the configuration and flight profile should be performed. The specification of the aircraft configuration is a detailed and nonlinear process, however, and might in principle change for each of the four scenarios described in section 2. Therefore, to simplify the analysis, the optimisation was carried out in two phases. In the first phase, a coupled aircraft-flight profile design procedure was carried out for a baseline mission akin to the CI scenario, to ensure the feasibility of the entire interval of possible operating scenarios considered here (DSE Group 02 2016). In the second phase, the aircraft configuration was held fixed and the flight profile re-optimised for each of the four scenarios in turn. The coupled optimisation procedure is a loop of manually interconnected design tools (Lukaczyk et al. 2015; Drela and Youngren 2004; Cavagna et al. 2011; Visser 2015); its detailed description is included in the supplementary material.

The result of the first optimisation phase was an unusual aircraft configuration capable of carrying a large fuel and payload mass to stratospheric altitudes. This can be expected to be close to the fully optimal configuration for each of the four scenarios, as each scenario is constrained by the same critical flight phase. In scenarios where dispersion rates are higher, flights can be shorter and less fuel is required. This in turn allows more payload to be carried per flight, reducing the annual number of flights. However, even the lowest number of flights required was found to be substantial, favouring the use of a specially designed aircraft capable of carrying a large fuel and payload mass in all four scenarios.

In summary, the two-phase optimisation approach described above is advantageous in that it allows for a more straightforward comparison of the scenarios. It is also more realistic, in that the ultimate choice of scenario is likely to be made after the aircraft is in service and long-term effects of SAI have been quantified.

#### 4.1 Results of the first stage of optimisation

This section describes the baseline aircraft configuration which emerged from the first phase of the optimisation procedure. Within this procedure, the remaining systems required for operation—the fuel, hydraulic, electrical, communications, hardware and software and data handling systems—were also developed to the preliminary stage. These largely mirror implementations in conventional modern aircraft and were not found to significantly influence the main optimisation process. The reader is referred to (DSE Group 02 2016) for a more detailed description of these systems. The baseline aircraft configuration is illustrated in Fig. 2 and presented in Table 1.

The unusual aspects of the baseline aircraft configuration are almost entirely the result of high-altitude and high-payload requirements. It features a large and slender wing, with a supercritical airfoil designed to provide high lift at high Mach numbers. Four custom turbofan engines, each rated to supply 26 kN of thrust at 20 km altitude, are used to overcome the relatively high drag associated with stratospheric operations, while simultaneously capable of supplying up to 2 MW of power to heat and evaporate  $H_2SO_4$ . This number assumes  $H_2SO_4$  is heated on the ground and maintained at a temperature close to its boiling point until it is evaporated.  $H_2SO_4$  is stored in cross-linked polyethylene (XLPE) tanks in the



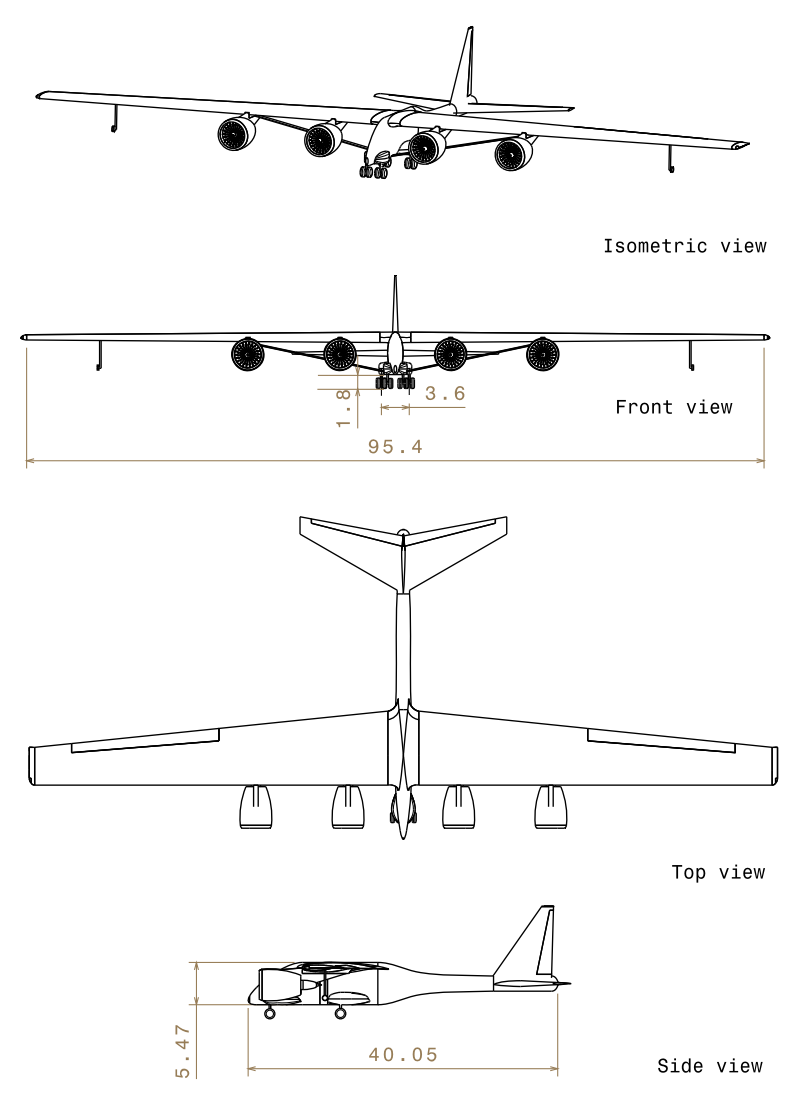


Fig. 2 Isometric view and three projection view of the proposed stratospheric aerosol delivery aircraft. Dimensions are in metres

wings (PolyProcessing 2013; R.A.W. Corporation 2019). At the maximum  $114 \, \mathrm{kg \, s^{-1}}$  injection rate prescribed by the third scenario of Section 2, an aerosol outlet cross sectional area interval between  $10 \, \mathrm{cm^2}$  and  $100 \, \mathrm{cm^2}$  results in injection velocities between approximately 2 and  $0.2 \, \mathrm{ms^{-1}}$ . These are practically attainable numbers that are unlikely to influence engine performance. It will thus be assumed that only one outboard engine, constantly operating at a relatively high thrust value, will be used for aerosol injection. This prevents suboptimal aerosol growth conditions by interaction between multiple expanding plumes. In addition, the use of only one outboard plume minimises the risk of corrosive  $H_2SO_4$  impinging on outer aircraft surfaces. Still, corrosion-resistant coatings are used where necessary on aircraft surfaces and especially engine outlet surfaces.



Table 1 Baseline aircraft design parameters

Design parameter (unit)	Value		
Diversion cruise (km)	1000		
Delivery cruise altitude (km)	20.0-20.5		
Take-off weight (tons)	150		
Operational empty weight (tons)	102		
Delivery cruise speed (ms <sup>-1</sup> )	210		
Delivery cruise stall speed (ms <sup>-1</sup> )	191		
Wing reference area (m <sup>2</sup> )	700		
Wing aspect ratio (-)	13.0		
Wing airfoil	NASA SC(2)-0714 (Jenkins 1989)		
Custom engine equivalent sea-level thrust at design condition (kN)	383		
Custom engine inlet diameter (m)	3.50		
Specific fuel consumption, 20 km (kg N <sup>-1</sup> s <sup>-1</sup> )	$1.56 \cdot 10^{-5}$		
Wing box weight (kg)	28,000		
Wing box material	Boron-fibre		
	composite		
Strut length (m)	19.9		
Control system	Unmanned,		
	autonomous		
Payload tank material	XLPE		

The first three scenarios described in Section 2 necessitate the use of an evaporation system to ensure the  $H_2SO_4$  is injected as a condensable gas, which in turns requires engine power. The engines are sized for critical flight phases, as will be outlined in Section 4.2, whereas aerosol is dispersed in flight segments during which thrust demand is much lower. Hence, there is sufficient excess engine capacity for aerosol evaporation and temperature control during dispersion segments. Aerosol evaporation will take place at the aerosol outlets, in order to allow the formed gas to expand.

The wings are sufficiently spacious to accommodate the full interval of payloads and fuel considered in this study, allowing a small, slender fuselage. A boron-fibre composite wing box supported by telescopic struts is used to achieve a relatively high aspect ratio while avoiding aeroelastic modes by margins of at least 50 ms<sup>-1</sup> relative to standard operating conditions. Compliance with load cases throughout the flight envelope was verified, following the requirements of EASA CS 25 for the certification of large aircraft.

The aircraft is operated unmanned, following a programmed mission and when necessary operated remotely from ground stations. This is mainly due to the very low air densities encountered in the stratospheric parts of its operation, for which maintaining a suitable onboard crew environment imposes a significant weight penalty and reduces the number of feasible aircraft layout choices. In addition, the scale of the mission and necessity for crew redundancy requires a large number of pilots, each with high training and employment costs. In contrast, one ground operator can simultaneously control several unmanned aircraft, if only one of these is in a critical flight phase. Unmanned aircraft introduce several additional requirements, however, including the need for complex redundant automated control systems. Ground stations with specialised technical equipment must also be established and



maintained. Overall however, a substantial economic benefit can be gained from unmanned operation.

The development and production time required for a fleet of the above aircraft is estimated to be between six to nine years (DSE Group 02 2016). This is based on estimates for high-payload transport aircraft and modern airliners (Spitz et al. 2001), as well as production rate buildup for such aircraft (Flottau 2015; McClellan et al. 2010) and the time required for the development of state-of-the-art high-bypass turbofan engines.

## 4.2 Results of the second stage of optimisation

## 4.2.1 Scenario operational characteristics

Modern air traffic regulations specify a minimum distance of 3 nautical miles between consecutive departures of heavy aircraft (Rooseleer and Treve 2015). At take-off and landing speeds of the proposed aircraft, this results in a minimum delay of slightly less than a minute when appropriate margins are accounted for, allowing slightly over 1500 flights per day per airport. The *CI* scenario can then be carried out with four airports. For the remaining scenarios which require fewer flights, the use of four airports has also been assumed in order to ensure one airport per hemisphere and one for redundancy. For a more extreme range of operations, as will be considered in Part 2 of this study, airports are added as needed if more flights per day than in the *CI* scenario are required. In all cases, airports will be placed at a latitude where the injection is centred around the target latitudes of 15° N and S. It is assumed that existing airports with a 2500 m or longer runway are used.

For H<sub>2</sub>SO<sub>4</sub> injection scenarios, the flight lengths needed to achieve the design dispersion rates can be substantial, demanding a dedicated flight profile. This will be directed along meridional tracks, such that round-trip flights are advantageous compared with transit flights in order to contain the required number of airports and facilitate injection perpendicular to the fastest advection dimension around a specified latitude. Each of the H<sub>2</sub>SO<sub>4</sub> injection scenarios are thus divided into two legs. The outbound leg is oriented in the local poleward direction (south in southern hemisphere, north in northern hemisphere). After climbing to an altitude of 20 km, aerosol delivery is initiated. At the mid-flight point, the aircraft turns to a reciprocal heading and then climbs to 20.5 km. The remaining aerosol is then delivered at this higher altitude on the return leg. The more extreme return operating condition is facilitated by weight reduction due to fuel burn and aerosol dispersion on the outbound leg. To minimise plume interactions which could affect particle size development, consecutive flights are performed on the same meridional track. The plumes from consecutive flights at the same altitude are assumed to be separated relatively quickly by stratospheric winds, which are generally zonal and thus perpendicular to meridional tracks; this forms the rationale for orienting the flight profiles along meridians. Additional plume separation between outbound and inbound aircraft is provided by the altitude difference between the legs. Nowhere in the envelope of plume diffusivity and stratospheric zonal winds considered here do the plumes begin overlapping in the early growth phase of sulphate aerosols, assuming consecutive aircraft are spaced by existing air traffic regulations.

For the  $SO_2$  scenario, plume interactions are irrelevant and flight orientation can be arbitrary. In this case each flight is assumed to be relatively short, consisting of the time required for take-off and climb to 20 km, the time required for a high-rate dispersal of the payload at this altitude and the time required for descent and landing.



Scenario	CI	FI	OFI	SO <sub>2</sub>
Payload type	H <sub>2</sub> SO <sub>4</sub>	H <sub>2</sub> SO <sub>4</sub>	H <sub>2</sub> SO <sub>4</sub>	SO <sub>2</sub>
Annual injection (Mt year <sup>-1</sup> )	15	15	15	20
Diffusivity (m <sup>2</sup> s <sup>-1</sup> )	$10^{2}$	$10^{2}$	$3 \cdot 10^2$	_
Initial concentration (# cm <sup>-3</sup> )	$10^{16}$	$10^{16}$	$3\cdot 10^{17}$	_
Bypass injection	No	Yes	Yes	_
Altitude (km)	20-20.5	20-20.5	20-20.5	20
DR (kg m <sup>-1</sup> )	0.0020	0.017	0.54	3.0
Payload/flight (tons)	6.80	21.1	28.9	29.6
Delivery range (km)	3370	1230	53.1	10.0
Fuel/flight (tons)	30.9	16.7	8.94	8.12
Airports	4.00	4.00	4.00	4.00
Flights/day	6000	2000	1400	1900
Fleet size	2400	480	230	290

Table 2 Main operational aspects of the delivery scenarios

## 4.2.2 Optimised flight profiles

The bottom half of Table 2 presents the operational parameters for the four delivery scenarios resulting from the second optimisation phase. The flight profiles for each scenario consist of the in- and outbound delivery range, as well as a 1000 km diversion range at low altitude (11 km), which allows redirecting aircraft to different airports in case of emergency.

To illustrate the main aspects of the analysis, the results for the CI scenario are now described in detail. Figure 3a and b display the aircraft's altitude profile and its weight

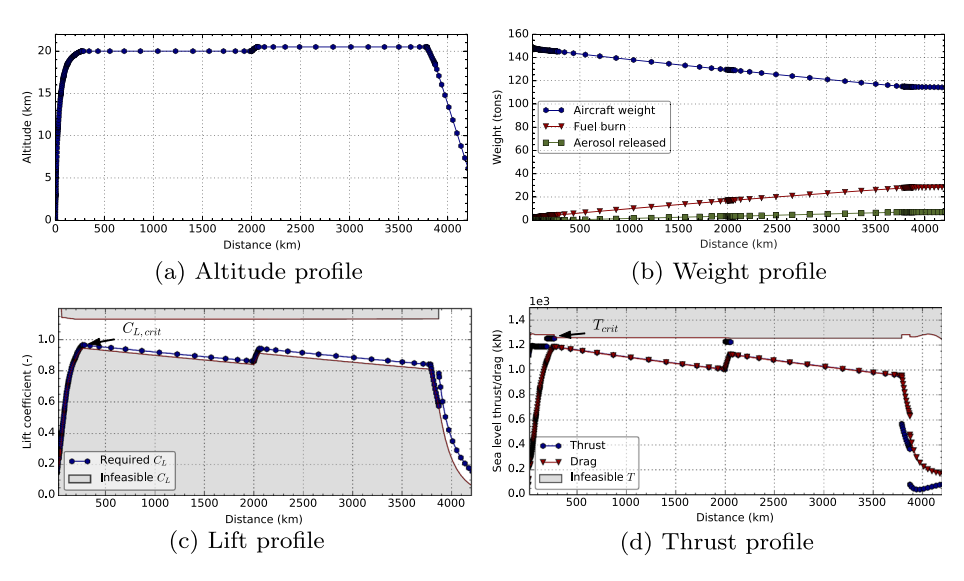


Fig. 3 Aircraft performance parameters during a flight of the *CI* scenario



distribution during the flight. The outbound delivery leg of 1680 km is flown at 20 km altitude, releasing sufficient aerosol and fuel to allow the lightened aircraft to climb to 20.5 km where the returning delivery leg is flown. The dispersion rate is held constant throughout the delivery range. The complete flight description includes a throttle setting distribution and changes to the aerodynamic configuration.

Figure 3c and d highlight how the end of the climb to the initial stratospheric delivery altitude (after approximately 250 km) presents a critical condition that constrains and drives the aircraft design. Here the aircraft operates close to the coffin corner. In Fig. 3c, this is the point where  $C_L = C_{L,crit}$ , corresponding to  $V_{crit}$  in Fig. 1b, where the aircraft must negotiate the narrow range between 191 and 212 m/s, the stall and drag divergence limits. In this condition both the induced drag and airfoil section drag due to drag divergence are high. For the proposed configuration, it is generally better to operate at the higher end of this speed range (at lower  $C_L$ ) as the penalties associated with induced drag are larger than those associated with drag divergence.

In any case, the net drag at the critical condition is very high. The engines must balance this drag, while providing additional thrust to maintain a sufficient climb rate. This point thus sets the critical thrust requirement ( $T_{crit}$ ) for the engines. For the proposed configuration, a total of 1250 kN of equivalent sea-level thrust is required at 20 km altitude, including margins for off-design atmospheric conditions. This critical thrust level must only be provided for a short interval in time, since after this point the climb is arrested and aerosol delivery and fuel burn act to reduce the weight and required  $C_L$ . For the proposed design  $T_{crit}$  is provided using four custom engines operating at 97.5% throttle and high turbine inlet temperatures. To avoid unforeseeable maintenance cost increases, this condition is allowed to be maintained for an interval of no more than five minutes, corresponding to the time commercial airliners are normally allowed to deploy maximum take-off thrust (Roskam 1985). Later in the flight (near 2000 km), a short  $T_{crit}$  interval is again employed to climb to the more extreme return leg altitude.

The other two  $H_2SO_4$  injection scenarios, FI and OFI, feature similar flight profiles in concept and constraints, with increased payload weights and lower fuel weights and distances. In contrast, the optimised  $SO_2$  injection scenario is simpler, in that it only consists of a climb to 20 km altitude, the quick release of all payload and return to the airport.

Despite the similarities in their layout, the four scenarios differ substantially in their operational parameters. Table 2 reveals a rapid increase in the scale of the operation as DR decreases, with the CI scenario requiring a fleet that is a full order of magnitude larger than the OFI and  $SO_2$  scenarios. While we judge all scenarios to remain inside the frame of what can be technologically and logistically achieved, it can be anticipated that delivery scenarios that lean in the direction of the OFI scenario will have a considerably lower costs and emissions than the other scenarios. This will be quantified in Part 2 of this series.

## 5 Consequences of alternative design options

The delivery system presented in the previous sections depends on a number of assumed design options. In this section we briefly summarise the consequences resulting from modifications to the options which most strongly influence the configuration and operation of the proposed aircraft, namely the propulsion system and the operating altitude. These two aspects fundamentally change the aircraft's critical design condition, leading to non-linear



downstream effects which frame the operation's costs and emissions. In order to avoid compounding the uncertainties associated with the achievement of the FI and OFI scenarios, the design changes are only presented for the CI scenario. The general conclusions can be anticipated to be similar for the remaining scenarios, although the specific quantitative effects will differ. The supplementary material of this paper contains an extensive, detailed discussion of the analysis of the alternate design options. The effects on the performance of the system are discussed here, while the resulting changes to financial costs and equivalent  $CO_2$  emissions are quantified in part 2 and its supplementary material, along with additional sensitivities arising from uncertainties in other design inputs.

## 5.1 Alternative propulsion systems

Two alternatives to the proposed custom engine based on existing engines were considered: F-100-PW-229 low-bypass turbofans (Camm 1993) and General Electric GE90-115B high-bypass turbofans (EASA 2017). Flight profile optimisation reveals that both alternatives increase the take-off weight of the aircraft. Hence, to negotiate the critical design condition, both alternatives require more engines; eighteen engines per aircraft for the F100 option and six engines per aircraft for the GE90 option.

The F100 alternative is inferior in the *CI* scenario. While a single F100 is considerably lighter than a custom engine, the high engine number only yields moderate savings in the aircraft's operating empty weight (OEW). Furthermore the much higher fuel consumption per unit thrust (specific fuel consumption, or SFC) increases the amount of fuel used per flight. This results in a lower payload-range combination, and consequently a higher number of flights and a larger fleet size.

Since six GE90s deliver considerably more thrust than four custom-design engines, this alternative is not constrained by  $T_{crit}$ , but by  $C_{L,crit}$ . At this constraint, the net result of the GE90 option is an increase in OEW, offsetting fuel savings due to lower SFC and obliging a lower payload-range combination, which in turn leads to increases in the fleet size and number of flights per day.

From this analysis can thus be concluded that neither of the alternative engine configurations considered here are likely to outperform the proposed custom engine in the CI scenario from an operational perspective. This was also found to be true for the other  $H_2SO_4$  injection scenarios.

## 5.2 Alternative cruise altitudes

Higher stratospheric delivery altitudes are beneficial for aerosol residence time and thus radiative effectiveness, although this is partly offset by less effective particles due to increased coagulation e.g., (Robock 2014; Rasch et al. 2008; Pope et al. 2012; Tilmes et al. 2017). Section 4.1 outlined the very narrow aerodynamic operating margin at capping thrust requirements at the top of the initial climb, making it difficult to change this mission segment without exceeding critical limits. Thus, higher altitudes can only be achieved with the current aircraft configuration by reducing payload or fuel and delivery range, making the aircraft lighter when it negotiates this climb.

Increasing the initial delivery altitude of the *CI* scenario by 0.5 km leads to extreme effects as it rapidly reduces payload and range, increasing the number of flights and fleet size accordingly. These increase by factors of 20 and 10, respectively, resulting in approximately 120,000 flights per day and 20,000 aircraft; unattainable numbers from a practical point of view. A complete quantitative overview can be found in the supplementary material.



#### 6 Conclusions and recommendations

This paper has considered the design of an SAI delivery system employing specialised aircraft. Due to the exceptional requirements involved, relatively detailed models of the aircraft's configuration and operation have been used to ensure the feasibility of the resulting design. As the operational efficiency of direct  $H_2SO_4$  injection is influenced by the achievable dispersion rate, three separate direct  $H_2SO_4$  injection scenarios were analysed. An additional scenario considering  $SO_2$  injection was also considered. All of the scenarios were unusual in that they required the delivery of large payloads to stratospheric altitudes. The direct  $H_2SO_4$  injection scenarios were additionally challenging in that they required substantial flight radii.

The resulting operating conditions necessitated the use of a coupled aircraft/flight profile design procedure. This produced a baseline aircraft and flight profile design, the latter part of which was re-optimised in a second design stage for each of the considered scenarios. The aircraft is specialised for carrying large fuel or aerosol masses to high altitudes, including features such as unmanned operation, a large, high aspect ratio wing and custom engines. The sensitivity of the design to delivery altitude was found to be high, precluding practical operation at altitudes substantially above 20 km when a substantial delivery range must be covered. The custom engines were shown to provide substantial benefits over the considered off-the-shelf alternatives. However, these benefits must be weighed against the costs the development of custom engines would incur. This trade-off will be examined in Part 2 of this series.

The second stage of the design produced optimised profiles for each scenario, allowing for estimates of their operational requirements for SAI with an equivalent negative radiative forcing of 2.5 to 3 W m $^{-2}$ . These indicate that the resources required for direct  $H_2SO_4$  injection are generally greater than those required for  $SO_2$  injection. However, the former were found to scale strongly with engine exhaust diffusivity, such that if optimised full engine exhaust injection is used, the required resources could be similar to those of  $SO_2$  injection. This indicates that investments directed towards achieving high engine exhaust diffusivities will likely provide substantial benefits if SAI is to be implemented.

**Open Access** This article is licensed under a Creative Commons Attribution 4.0 International License, which permits use, sharing, adaptation, distribution and reproduction in any medium or format, as long as you give appropriate credit to the original author(s) and the source, provide a link to the Creative Commons licence, and indicate if changes were made. The images or other third party material in this article are included in the article's Creative Commons licence, unless indicated otherwise in a credit line to the material. If material is not included in the article's Creative Commons licence and your intended use is not permitted by statutory regulation or exceeds the permitted use, you will need to obtain permission directly from the copyright holder. To view a copy of this licence, visit http://creativecommonshorg/licenses/by/4.0/.

**Publisher's note** Springer Nature remains neutral with regard to jurisdictional claims in published maps and institutional affiliations.

#### References

Benduhn F, Schallock J, Lawrence MG (2016) Early growth dynamical implications for the steerability of stratospheric solar radiation management via sulfur aerosol particles. Geophys Res Lett 43(18):9956–9963

Camm F (1993) The development of the F100-PW-220 and F110-GE-100 engines: a case study of risk assessment and risk management. Tech. rep., Rand Corporation



- Cavagna L, Ricci S, Travaglini L (2011) NeoCASS: an integrated tool for structural sizing, aeroelastic analysis and MDO at conceptual design level. Progress in Aerospace Sciences 47(8):621–635
- Clarke L, Jiang K, Akimoto K, Babiker M, Blanford G, Fisher-Vanden K, Hourcade J-C, Krey V, Kriegler E, Löschel A, et al. (2014) Assessing transformation pathways. In: Edenhofer O., et al. (eds) Climate Change 2014: Mitigation of Climate Change. Contribution of Working Group III to the Fifth Assessment Report of the Intergovernmental Panel on Climate Change. Cambridge University Press, Cambridge
- Cook J, Nuccitelli D, Green SA, Richardson M, Winkler B, Painting R, Way R, Jacobs P, Skuce A (2013)

  Quantifying the consensus on anthropogenic global warming in the scientific literature. Environ Res Lett 8(2)
- Crutzen PJ (2006) Albedo enhancement by stratospheric sulfur injections: a contribution to resolve a policy dilemma? Climatic change 77(3):211–220
- Davidson P, Burgoyne C, Hunt H, Causier M (2012) Lifting options for stratospheric aerosol geoengineering: advantages of tethered balloon systems. Phil. Trans. R. Soc. A. 370(1974):4263–4300
- Debiasi M, Dhanabalan S, Tsai HM, Papamoschou D (2007) Mixing enhancement of high-bypass turbofan exhaust via contouring of fan nozzle. In: 37th AIAA Fluid Dynamics Conference and Exhibit, p 4497
- Drela M, Youngren H (2004) Athena vortex lattice. 3
- DSE Group 02 (2016) A delivery system for stratospheric aerosol geoengineering, Delft University of Technology
- Dykema J, Keith D, Keutsch F (2016) Improved aerosol radiative properties as a foundation for solar geoengineering risk assessment. Geophys Res Lett 43(14):7758–7766
- EASA (2017) Type-certificate data sheet no. IM.E.002 for GE90 series engines
- Flottau J (2015) Airbus plans to increase A350 production rate to 13 per month. Retrieved from: http://aviationweek.com/paris-air-show-2015/airbus-plans-increase-a350-production-rate-13-month Accessed: 27/10/2018
- Heckendorn P, Weisenstein D, Fueglistaler S, Luo BP, Rozanov E, Schraner M, Thomason LW, Peter T (2009) The impact of geoengineering aerosols on stratospheric temperature and ozone. Environ Res Lett 4(4):108–120
- Holzman JK, Webb LD, Burcham FW Jr (1996) Flight and static exhaust flow properties of an F110-GE-129 engine in an F-16XL airplane during acoustic tests, NASA Dryden Flight Research Center
- IPCC (2013) Climate Change 2013: The Physical Science Basis. Contribution of Working Group I to the Fifth Assessment Report of the Intergovernmental Panel on Climate Change Stocker TF, Qin D, Plattner G-K, Tignor M, Allen SK, Boschung J, Nauels A, Xia Y, Bex V, Midgley PM (eds), Cambridge University Press
- IPCC (2018) Global warming of 1.5°C. An IPCC Special Report on the impacts of global warming of 1.5°C above pre-industrial levels and related global greenhouse gas emission pathways, in the context of strengthening the global response to the threat of climate change, sustainable development, and efforts to eradicate poverty Masson-Delmotte Valerie, Zhai P., Prtner Hans-Otto, Roberts Debra, Skea J., Shukla P., Pirani Anna, Moufouma-Okia Wilfran, Pan C., Pidcock R., Connors S., Matthews Robin, Chen Y., Zhou X., Gomis Melissa, Lonnoy E., Maycock T., Tignor M., Waterfield T. (eds), Cambridge University
- Jenkins RV (1989) NASA SC(2)-0714 airfoil data corrected for sidewall boundary-layer effects in the Langley 0.3-meter transonic cryogenic tunnel, NASA Langley Research Center
- Keith DW, Weisenstein DK, Dykema JA, Keutsch FN (2016) Stratospheric solar geoengineering without ozone loss. Proc Natl Acad Sci 113(52):14910–14914
- Larkin M, Blatt J (1984) Energy efficient engine exhaust mixer model technology report addendum; phase 3 test program, NASA Lewis Research Center
- Lukaczyk T, Wendorff AD, Botero E, MacDonald T, Momose T, Variyar A, Vegh JM, Colonno M, Economon TD, Alonso JJ (2015) SUAVE: An Open-Source Environment for Multi-Fidelity Conceptual Vehicle Design:3087
- MacMartin DG, Kravitz B, Tilmes S, Richter JH, Mills MJ, Lamarque J-F, Tribbia JJ, Vitt F (2017) The climate response to stratospheric aerosol geoengineering can be tailored using multiple injection locations. J Geophys Res Atmos 122(23):12–574
- McClellan J, Sisco J, Suarez BGK (2010) Geoengineering cost analysis final report, Aurora Flight Sciences Mundt C, Lieser J (2001) Performance improvement of propulsion systems by optimization of the mixing efficiency and pressure loss of forced mixers. In: European propulsion Forum "Affordability and Environment-Key Challenges for Propulsion in the 21st Century
- Pierce JR, Weisenstein D, Heckendorn P, Peter T, Keith DW (2010) Efficient formation of stratospheric aerosol for climate engineering by emission of condensible vapor from aircraft. Geophys Res Lett 37(18):L18805
- PolyProcessing (2013) Chemical storage tank systems and accessories: product and resource guide



- Pope FD, Braesicke P, Grainger RG, Kalberer M, Watson IM, Davidson PJ, Cox RA (2012) Stratospheric aerosol particles and solar-radiation management. Nat Clim Change 2(10):713–719
- Rasch PJ, Tilmes S, Turco RP, Robock A, Oman L, Chen C-C, Stenchikov GL, Garcia RR (2008) An overview of geoengineering of climate using stratospheric sulphate aerosols. Phil. Trans. R. Soc. A. 366(1882):4007–4037
- R.A.W. Corporation (2019) Why polyethylene? Retrieved from: http://www.rawtanks.com/technical-specs/ why-polyethylene.html. Accessed: 03/03/2019
- Reed RJ (1966) Zonal wind behavior in the equatorial stratosphere and lower mesosphere. J Geophys Res 71(18):4223–4233
- Robock A (2014) Geoengineering of the climate system, stratospheric aerosol geoengineering. Issues in Environmental Science and Technology. The Royal Society of Chemistry
- Rooseleer F, Treve V (2015) ReCaT-EU European wake turbulence categorisation and separation minima on approach and departure. Tech rep., Eurocontrol
- Roskam J (1985) Airplane design VII: determination of stability, control and performance characteristics: Far and military requirements. DARcorporation
- Schumann U, Schlager H, Arnold F, Baumann R, Haschberger P, Klemm O (1998) Dilution of aircraft exhaust plumes at cruise altitudes. Atmos Environ 32(18):3097–3103
- Shepherd JG (2009) Geoengineering the climate: science, governance and uncertainty. Project Report
- Smith JP, Dykema JA, Keith DW (2018) Production of sulfates onboard an aircraft: implications for the cost and feasibility of stratospheric solar geoengineering. Earth Space Sci 5(4):150–162
- Smith W, Wagner G (2018) Stratospheric aerosol injection tactics and costs in the first 15 years of deployment. Environ Res Lett 13(12)
- Spitz W, Berardino F, Golaszewski R, Johnson J (2001) Development cycle time simulation for civil aircraft, NASA Langley Research Center
- Tilmes S, Richter JH, Mills MJ, Kravitz B, MacMartin DG, Vitt F, Tribbia JJ, Lamarque J-F (2017) Sensitivity of aerosol distribution and climate response to stratospheric SO2 injection locations. J Geophys Res Atmos 122(23)
- Torenbeek E (2013) Advanced aircraft design. Wiley, New York
- Turco RP, Yu F (1997) Aerosol invariance in expanding coagulating plumes. Geophys Res Lett 24(10):1223–1226
- Uppala SM et al (2005) The ERA-40 re-analysis. Q J R Meteorol Soc 131(612):2961–3012
- Vattioni S, Weisenstein D, Keith D, Feinberg A, Peter T, Stenke A (2019) Exploring accumulation-mode H2SO4 versus SO2 stratospheric sulfate geoengineering in a sectional aerosol-chemistry-climate model. Atmospheric Chemistry and Physics 19(7):4877–4897
- Visser WPJ (2015) Generic Analysis Methods for Gas Turbine Engine Performance: The development of the gas turbine simulation program GSP
- Weisenstein D, Keith D, Dykema J (2015) Solar geoengineering using solid aerosol in the stratosphere. Atmos Chem Phys 15(20):11835–11859
- Yu F, Turco RP (1998) The formation and evolution of aerosols in stratospheric aircraft plumes: numerical simulations and comparisons with observations. J Geophys Res Atmos 103(D20):25915–25934

